1989

A Fast Moving Knot of Radio Emission in the Active Galaxy NGC 1275

Jonathan M. Marr
Haverford College, jmarr@haverford.edu

THE ASTROPHYSICAL JOURNAL, 337:671–679, 1989 February 15

A FAST-MOVING KNOT OF RADIO EMISSION IN THE ACTIVE GALAXY NGC 1275

J. M. MARR, D. C. BACKER, AND M. C. H. WRIGHT
Radio Astronomy Laboratory and Astronomy Department, University of California, Berkeley
AND
A. C. S. READHEAD AND R. MOORE
Astronomy Department, California Institute of Technology
Received 1988 March 24; accepted 1988 August 3

ABSTRACT

We have mapped the nearby ($z = 0.018$) active galaxy NGC 1275 (3C 84) at six different epochs from 1981 to 1986 at 1.3 cm (22.3 GHz) with a global VLBI array of seven telescopes. In this paper we describe a long-lived knot of emission separating from the main radio component with a projected velocity of $0.49 \pm 0.10h^{-1}c$. This knot moves through diffuse emission that also moves away from the main component with a slower projected velocity of $0.33 \pm 0.13h^{-1}c$.

We show that the knot and diffuse emission are associated with flux-density increases that occurred around 1968 and 1959, respectively. We discuss the observations in terms of a core-jet model and propose that the jet collimation has increased over the lifetime of the present activity.

Subject headings: galaxies: individual (NGC 1275) — galaxies: nuclei — galaxies: Seyfert — galaxies: structure — interferometry — radio sources: galaxies

I. INTRODUCTION

The peculiar active galaxy NGC 1275 contains at its center the variable compact radio source 3C 84. The radio source has been shown to exhibit subluminal expansion of complex structure in a series of seven VLBI observations at 2.8 cm (10.7 GHz) from 1972 to 1982 (Schilizzi *et al.* 1975; Pauliny-Toth *et al.* 1976; Preuss *et al.* 1979; Romney *et al.* 1984). The images show a distinct northern component with amorphous emission to the south. In the earliest (low-sensitivity) images the source spans about 5 mas, and the southern emission is dominated by two peaks aligned with the northern component at $-9°$. In the later maps the full extent of the source has expanded to about 10 mas, and the southern structure is both diffuse and distributed roughly in a cone whose opening angle is about 20°. Romney *et al.* (1982) fitted a linear expansion rate of 0.34 ± 0.06 mas yr^{-1} to these data. This rate corresponds to a projected speed of $0.28 \pm 0.05h^{-1}c$ ($h = H/100$ km s^{-1} Mpc^{-1}) and implies a time of origin about 1961. Romney *et al.* (1984) interpret their results in terms of a core-jet model. They locate the core in the northernmost component and argue that it ejects matter bidirectionally close to the line of sight; Doppler enhancement of the emission from the material approaching us and Doppler attenuation of the emission from the counter ejecta produce the one-sided appearance. Symmetrical emission observed on larger scales and at lower frequencies (Noordam and de Bruyn 1982; Perley 1986) lends support to the bidirectional flow model.

O'Dea, Dent, and Balonek (1984, hereafter ODB) present flux-density variation curves of 3C 84 from monitoring at five radio frequencies between 1962 and 1982. A slowly evolving outburst is exhibited in the data at 15.5, 7.9, and 2.7 GHz (reproduced in Fig. 2 and discussed later). ODB present a model of the outburst consisting of expanding homogeneous synchrotron components with a time of origin of 1959. Their components correspond to those mapped in the VLBI images of Romney *et al.* (1984).

Unwin *et al.* (1982) present a spectral index map based on 5.0 and 10.7 GHz VLBI observations that show that the northern component has the most inverted spectrum in the source, in support of the interpretation of Romney *et al.* (1984). Unwin *et al.* (1982) also reveal a second region with an inverted or flat spectrum at the eastern edge of the southern diffuse emission.

Readhead *et al.* (1983) mapped NGC 1275 with VLBI at 1.3 cm (22.2 GHz) in 1981 April. They found a flux-density distribution similar to that seen at 2.8 cm, and noted the presence of a compact knot of emission in the southernmost component, which may coincide with the inverted-spectrum knot in the map of Unwin *et al.* (1982).

We present five succeeding 1.3 cm VLBI images from observations made in 1981–1986 along with the map of Readhead *et al.* (1983). In comparison with the 2.8 cm images of Romney *et al.* (1984), our time series of 1.3 cm maps displays the movement of the smaller and higher opacity regions of NGC 1275. The identification and movement of a compact knot are presented in § III. We discuss the relation of this knot to the jet in § IV. Properties of the bright core will be discussed in a later paper.

II. OBSERVATIONS

We observed NGC 1275 at 1.3 cm (22.2 GHz) with a global VLBI network at six epochs from 1981 to 1986. We observed at each epoch with the Mk II VLBI system, a bandwidth of 2 MHz, left-circular polarization, and six to seven global network telescopes. We correlated the raw data on the CIT–JPL processor using a coherent integration time of 2 minutes. This period gave negligible loss of coherence and provided good sensitivity on long baselines, where fringe amplitudes are weak. We calibrated the data *a priori* from ratios of antenna gains to system temperatures. The antenna gains were determined from antenna temperatures measured every half-hour at most stations and from gain curves for the others. The system temperatures were measured every half-hour at all stations. Table 1 gives a journal of the observations.

TABLE 1A

OBSERVATION PARAMETERS

EPOCH	ARRAY[a]	DURATION (hr)	TOTAL FLUX: Single Dish (Jy)	TOTAL FLUX: In Map (Jy)	PEAK FLUX (Jy beam^{-1})	SNR	NOTES
1981 Apr 2	BKGCYO	12	50.0	47.1	3.77	10	1
1981 Dec 2	BKGCYO	14	53.0	49.8	5.63	10	
1984 Oct 6	BSKGYO	12	44.5	43.2	3.18	10	2
1985 Feb 6	BSKNGYO	23	44.3	37.3	2.67	76	
1985 Oct 1	BSKNGYO	20	44.1	37.6	2.56	75	1
1986 Feb 27	BSKNGYO	16	45.0	39.7	3.27	74	3

NOTES.—(1) Bad weather during much of observation at some stations. (2) Limited data set: 15–20 minutes of data each hour of observation. (3) Limited long-baseline data: 5 hr of data on baselines 250 × 10^6 wavelengths.
[a] See Table 1B for explanation of symbols.

TABLE 1B

STATION PARAMETERS

Symbol	Station	Typical T_{sys} (K)	DIA (m)	Gain (K Jy^{-1})
B	Effelsburg	70	100	0.6
C	Algonquin	500	46	0.08
G	Green Bank	70	43	0.11
K	Haystack	90	37	0.104
N	Maryland Point	250	26	0.065
O	Owens Valley	70	40	0.12
S	Onsala	120	20	0.06
Y	VLA	120	25	0.04

Each data set was processed with the Caltech VLBI software package using the hybrid mapping routine with closure phases, closure amplitudes, and CLEAN (Readhead and Wilkinson 1978; Readhead *et al.* 1980). In the initial few iterations we mapped only the northern "core" region, 4 square mas, using only closure phases and continuing for 100–500 CLEAN components. The final image of the previous epoch was used as the input model for the first self-calibration. Next we opened the CLEAN window and continued processing to larger numbers of CLEAN components, reaching 2000–5000 by about the tenth iteration. Once the window contained all the expected structure, closure amplitudes were included in the self-calibration, excluding the shortest baselines at first. We initially allowed only a constant gain correction factor for each telescope in the closure amplitudes. As the rms fit of the model to the data approached twice the mean data noise error, we introduced shorter correction time scales. In the last iteration we allowed for point-by-point (2 minute) variations. In the 1985 and 1986 data we were able to find models that fitted to within ≤ 1.3 times the mean error bar in the raw data, with amplitude gain correction factors of 17% or less with time scales of ≥ 10 minutes. Some epochs needed recalibration using constraints given by *uv* crossing points, comparisons with other epoch data, and fits to the hybrid maps. The pointing of some antennas drifted on time scales as short as a half-hour; this was corrected in the recalibration.

The mapping process was verified by comparing two paths using different initial models (one contained just the core, and the other included diffuse structure to the south). They yielded the same structure above the 5% (or less) contour. However, the contour levels of large-scale structure below the 10% contour, although well above the noise in the maps, vary in structure from epoch to epoch. These lower contours may be sensitive to data errors that are not removed by self-calibration. Additionally, preliminary maps made in the AIPS package, where a number of CLEAN windows and restarting of CLEAN are allowed, indicate that the lower brightness structure is not mapped well in the Caltech package. These lower contours define the more diffuse emission, which is better stuided at longer wavelengths. We use our 1.3 cm images in this paper to study only the brighter, compact components and refer to the 2.8 cm images of Romney *et al.* (1984) for the diffuse structure.

The dynamic range of the 1981 April map (Readhead *et al.* 1983) was limited by the poor weather that occurred during much of the observation. The 1981 December map does not fit the data especially well and is considered only for confirmation of structure seen in the other maps. The 1984 October image results from 20 minutes of calibration data every hour that was recorded by A. Marscher during an observation of NRAO 140. The remaining three maps—1985 February, 1985 October, and 1986 February—are the most complete and are considered with the highest weights. Of these, the 1985 February map is the most reliable. Bad weather occurred at some stations in the 1985 October observation, and the 1986 February data contain just 5 hr of data on baselines longer than 250 × 10^6 wavelengths.

Figure 1 displays our series of maps. We show only the contours at 10% or greater. The beam in each map is 0.5 × 0.3 mas with a position angle −30°. One milliarcsecond corresponds to $0.26h^{-1}$ pc.

III. ANALYSIS

The compact northern component is more prominent in our 1.3 cm maps than in the 2.8 cm maps of Romney *et al.* (1984).

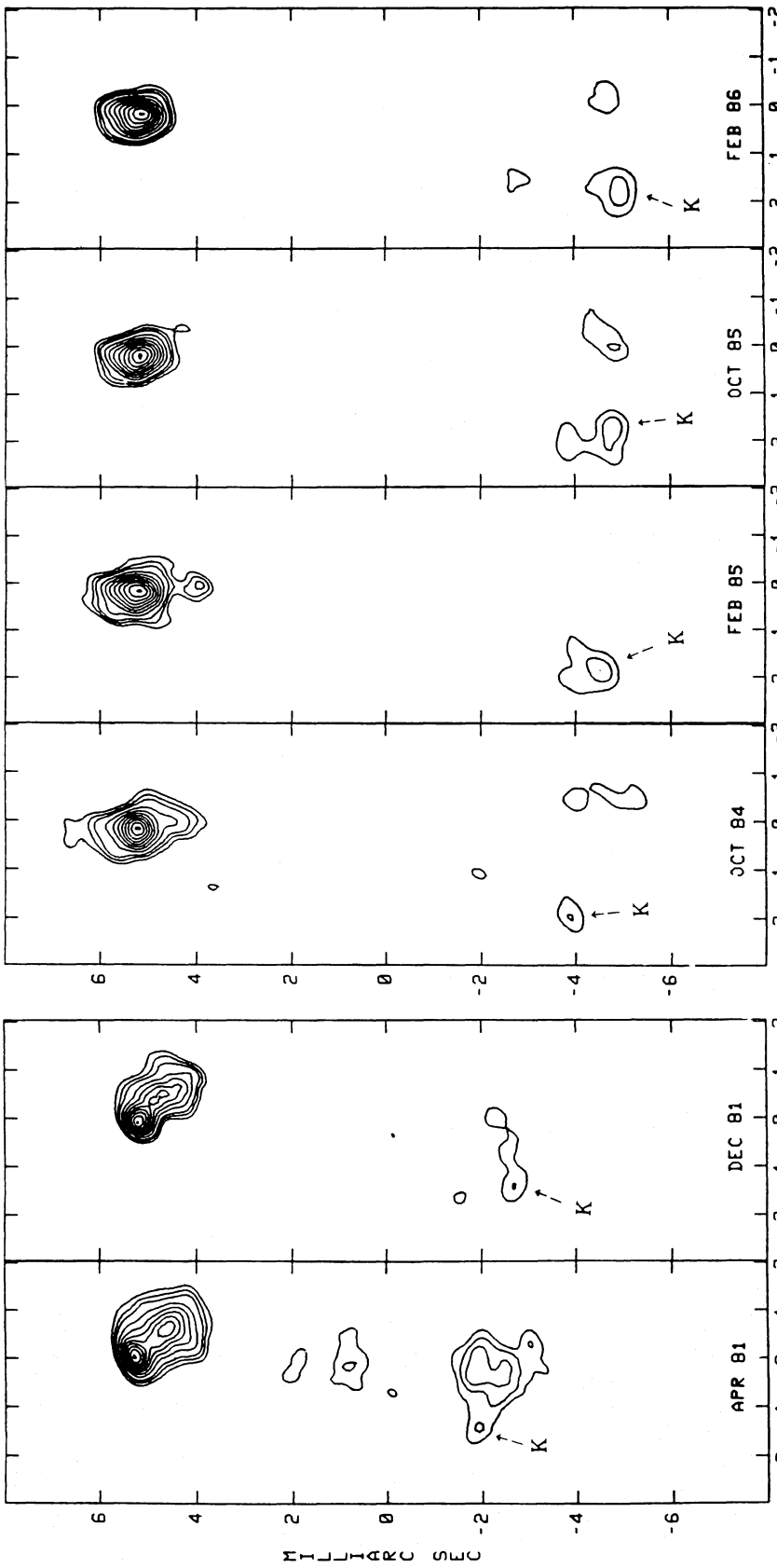

FIG. 1.—Series of 1.3 cm VLBI maps of NGC 1275 are shown at each epoch. The knot, labeled K, is referred to in the text. The displayed contours are −15%, −10%, 10%, 15%, 20%, 30%, 40%, 50%, 60%, 70%, 80%, 90%, and 99% of the peak. The CLEAN beam is 0.5 × 0.3 mas with a position angle of −30°.

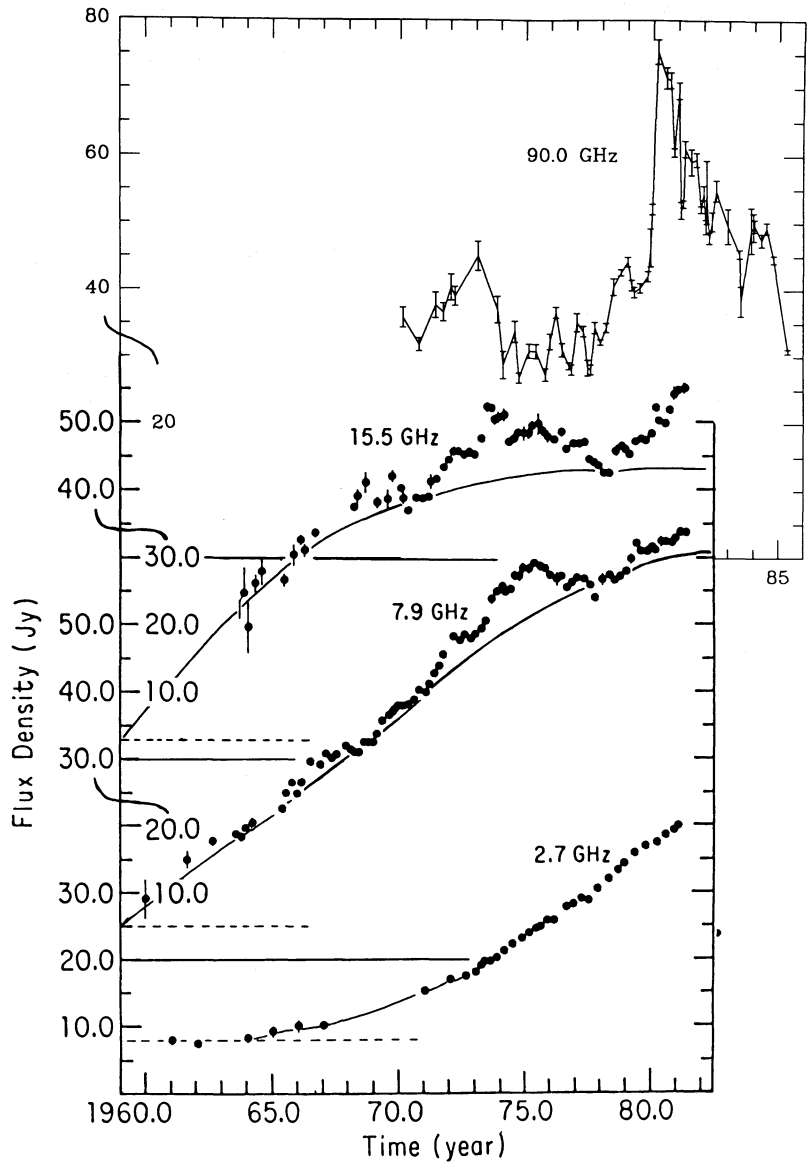

FIG. 2.—Flux-density variation curves of 3C 84 from O'Dea, Dent, and Balonek (1984) at 2.7, 7.9, and 15.5 GHz, and from Dent *et al.* (1983) at 90.0 GHz. The 90.0 GHz data were supplemented with an updated table provided by W. M. Kinzel (1986 private communication). The solid lines are drawn through the 2.7, 7.9, and 15.5 GHz data to distinguish between the slowly evolving outburst that originated in 1959 and the more rapidly evolving flares that have origins around 1970 and 1980. The zeros for each scale are represented by the solid horizontal lines, and the contribution from the large-scale, steep-spectrum component is shown as dashed horizontal lines.

The emission to the south has expanded over the 5 yr period; by 1986 the image spans about twice the size of the 1981 2.8 cm and 1.3 cm images (Fig. 1). Following Romney *et al.* (1984) and Unwin *et al.* (1982), we assume that the northern component corresponds to the core, or nucleus, of the galaxy and that the emission in the south has been ejected from the core.

We display in Figure 2 a composite of radio flux-density curves at four frequencies: those gathered by ODB, plus others by Dent *et al.* (1983) and W. M. Kinzel (1986, private communication). the curves reveal a slowly evolving outburst that has an origin time of 1959 (ODB). The appearance of the outburst at later times at lower frequencies supports the ODB model of expanding synchrotron components embedded in a thermally absorbing medium. Superposed on this outburst are a number of smaller flares. Below, we discuss these flares further.

At each epoch of our 1.3 cm data a compact knot is evident in the south. At most epochs the knot is the brightest point in the southern emission. The visibility data also support the identity of this knot: on the longest baselines the fringe amplitude displays beating between the knot and equally compact features in the core. We show in Table 2 the best-fit parameters to the knot obtained from model fits in the last four epochs. The flux density in the region around the knot was subtracted from each map, and the difference was subtracted as an input model for the model fits to the data. The knot's position in 1981 roughly coincides with the location of the inverted spectral region in the 1981 map by Unwin *et al.* (1982). We infer

TABLE 2

BEST-FIT MODELS OF KNOT (22.2 GHz)

Parameter	1984 Oct	1985 Feb	1985 Oct	1986 Feb
Flux (Jy)	1.0	0.5	1.4	1.4
Size (mas)	1.0	0.7	0.6	0.9

that the knot marks a small region of high density of relativistic particles.

The knot moves steadily southward with respect to the core. In Figure 3 we plot as filled circles the separation between the peak of the knot and the peak of the northern component as a function of time. The complex structure of the northern component complicates the interpretation of the peak position; we have no assurance that the peak of the flux-density distribution is a physically stable point. We have plotted as error bars the uncertainty in the absolute core center, allowing it to be anywhere within the 50% contour of the peak of the northern component. The error in measuring the peak-to-peak separations is represented by the size of the circles. The best linear fit to the separation data, shown as a dashed line in Figure 3, gives a projected velocity of 0.58 ± 0.12 mas yr^{-1}, corresponding to $0.49 \pm 0.10h^{-1}c$, and a time of zero separation of 1968.3 ± 3.2. The estimated errors in this fit were calculated by rotating the fitted line about the center point in the data and determining when the rms to the fit doubled. We note that there is a strong flare appearing at all frequencies in Figure 2 around 1970. We suggest that the appearance of the knot was associated with this flare event.

The fitted line in Figure 3 agrees with the data extremely well considering the structure confusion mentioned above. We infer that the knot and an emission feature in the core are long-lived and dominate the emission from the structure around them. The peak of the core emission appears steady enough in position that one may consider using it as a fiducial point in comparing maps.

Extrapolating the motion of the knot back to the epochs of the 2.8 cm images, we find that the expected positions of the knot in the 1979–1981 images lie in the southernmost component, while in the 1972–1976 images they coincide with the central (of three) components. The open boxes from 1972 to 1977 in Figure 3 mark separations in the 2.8 cm images of the bright central peak from the northern peak; from 1979 to 1981 the open boxes correspond to the northern-to-southern component separations. The error bars correspond to uncertainties in measuring the distances from the published maps. Romney *et al.* (1984) noted that the flux of the central 2.8 cm component appeared to have waned significantly by the 1979–1981 images.

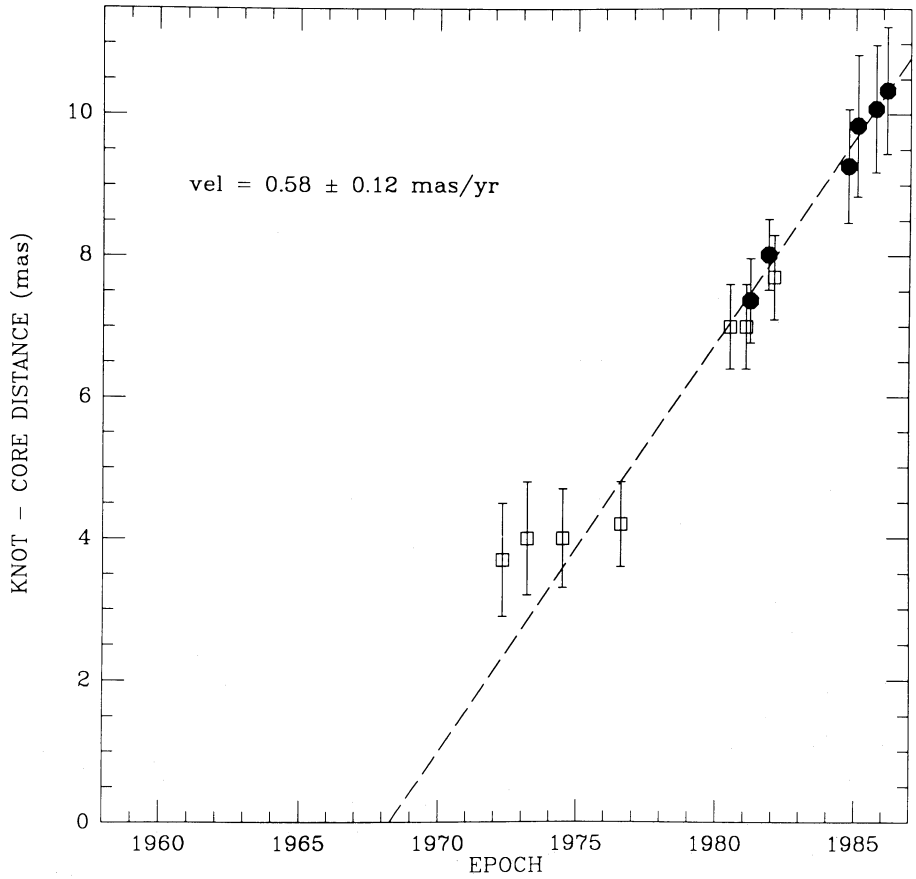

FIG. 3.—Distances of the knot from the core are plotted against time. Filled circles represent the distances in the six 1.3 cm images. The error bars, which correspond to the size of the 50% contour in the core, represent the uncertainty in the core position due to the complexity of the core structure. The dot size represents the error in the measurement of the peak-to-peak separations. The dashed line is a linear fit to the filled circles, $v = 0.58 \pm 0.12$ mas yr^{-1} $= 0.49 \pm 0.10h^{-1}c$. The open squares are the distances between the core and the component in each of the 2.8 cm images of Romney *et al.* (1982, 1984) that best fits the extrapolation of the fitted line.

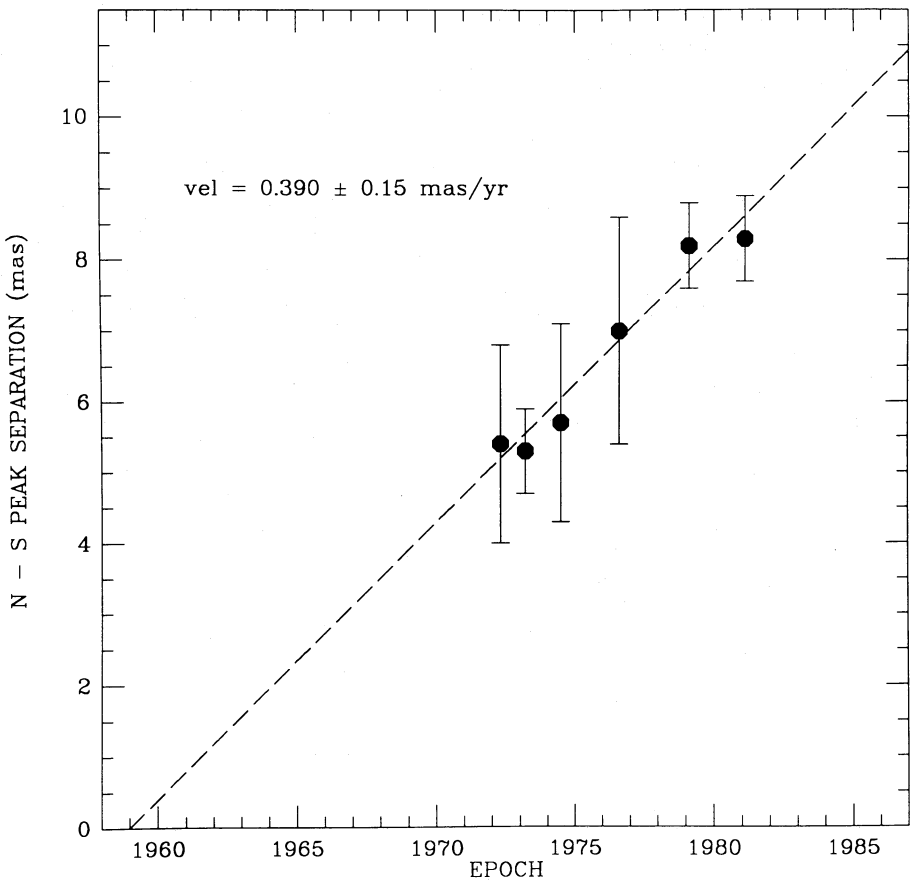

FIG. 4.—The entire size of the source, represented by the distance between the northernmost and southernmost peaks, is plotted against time. Filled circles represent the separation between the core and the southernmost peak in the 2.8 cm maps (Romney *et al.* 1982) where there is another peak past that extrapolated to be the knot. The error bars represent the uncertainty in identifying the correct peaks from the published 2.8 cm maps. The dashed line is a linear fit to the filled circles, $v = 0.39 \pm 0.15$ mas yr^{-1} $= 0.33 \pm 0.13h^{-1}c$.

We suggest that the central component in the early images contains the particles from the 1970 flare that now make up the knot, and that this component has moved into the southern component by the later images, leaving just diffuse emission behind.

The motion of the diffuse emission seen at 2.8 cm is exhibited in Figure 4, where we fit the expansion of the overall source size. We plot the measured separation against epoch between the center of the northern peak and the southernmost peak, past what we assume to be the knot. By 1981, the knot is close enough to the southern tip of the diffuse emission that identification of another peak past the knot is difficult. In order to separate the motion of the knot from that of the diffuse emission, we have not included these later epochs in the fit to the overall expansion of the source. The fitted distances are plotted as filled circles. We display error bars representative of the uncertainties in the peak positions. A linear fit gives a projected expansion velocity of the diffuse ejecta of 0.39 ± 0.15 mas yr^{-1} $(0.33 \pm 0.13h^{-1}c)$ and a time of origin of 1959.0 ± 6.8. We concur with Romney *et al.* (1984) that the diffuse emission was ejected in 1959 and is associated with the slowly evolving radio flux-density outburst seen in Figure 2.

IV. DISCUSSION

In the previous section we presented evidence for two separate components of ejection: a conal distribution of diffuse emission expanding from the core at 0.39 mas yr^{-1}, and a knot of emission moving at 0.58 mas yr^{-1} relative to the core in the same general direction. The error ranges for these velocities just overlap, but additional evidence from flux-density curves and the structure evolution strengthen the argument for distinct velocities. The appearance of the radio flux-density outburst (ODB) in 1959 coincides with the extrapolation of the diffuse emission's motion, while the knot's estimated motion is supported by the appearance of a radio flux-density flare shortly after the time of origin implied by the velocity. Additionally, the structure evolution depicted by combining the series of published 2.8 cm maps with out 1.3 cm maps supports the existence of two components with different velocities. We discuss in this section some physical parameters of the knot and the relevance of the standard hot spot model.

a) Physical Parameters

The spectral index map of Unwin *et al.* (1982) implies that the knot has a flat or inverted spectrum between 5 and 10.7 GHz. Model fits to data from observations at 22.2 GHz (Table 2), at 89 GHz by Backer *et al.* (1987), and at 43 GHz by Dhawan (1987) indicate that the flat spectrum of the knot extends to high frequencies. Although their accuracy is limited, these results also show that the knot's flux density certainly does not increase as rapidly as $\nu^{2.5}$, suggesting that the knot is not entirely opaque to synchrotron self-absorption.

If we assume that the knot is optically thin, we need an arbitrary cutoff to the electron energy density spectrum to avoid the infinite-energy problem. We estimate the magnetic field in the knot in this case, assuming equipartition of energy. The visibility curves show fringes that require 0.8 Jy to be contained within 0.7 mas at the knot. Assuming $\alpha = +0.9$ ($F_\nu \propto \nu^\alpha$), from Unwin *et al.* (1982), we estimate the magnetic field in the knot to be $B = 0.15h^{-2/7}$ G, following Miley (1980). This field yields a radiative lifetime of the synchrotron electrons of $3.1h^{3/7}$ yr. The estimate involves many assumptions: energy equipartition between the particles and the magnetic field and between the heavy and light particles, unity filling factor, homogeneous structure, upper and lower spectral cutoffs of 0.01 and 100 GHz, and $\langle \sin^2 \phi \rangle = \frac{1}{2}$, where ϕ is the angle between the field and the electron velocity vector.

Alternatively, as discussed by de Bruyn (1976), we can attribute the flat or inverted spectrum to nonuniform structure in the knot. The knot's physical parameters, such as density and magnetic field, may vary with radius, yielding an extended flat region of the synchrotron spectrum in the partially opaque regime. The spectral index, in this case, is determined by the dependence of optical depth and emissivity on radius. For example, a spherically symmetric synchrotron cloud with density depending on radius as $r^{-2.8}$ and magnetic field varying as $r^{-1.8}$ yields a spectrum like that observed by Unwin *et al.* (1982), $F_\nu \propto \nu^{+0.9}$ (de Bruyn 1976). We prefer this model over the optically thin model, since this scenario explains the observed spectrum without the need for an arbitrary electron-energy cutoff. Since the flux at a given frequency is dominated by the emission from the shell at the radius where the optical depth is of order unity, we assume that the emission at each frequency is dominated by a component at a spectral peak. Using the above parameters of the knot, a flux density of 0.8 Jy, and an angular size of 0.7 mas, we obtain a magnetic field estimate, following Marscher (1983), of 52 G. However, since this estimate depends sensitively on the angular size, $B \propto \theta^4$, and the value 0.7 mas is derived strictly from the resolution of the baselines showing the 0.8 Jy fringes, a smaller magnetic field is allowed. The Compton limit allows an angular size one-tenth of this value, since the brightness temperature for an angular size of 0.7 mas is only 10^{10} K. We can determine the expected size of the source by again assuming equipartition of energy (Scott and Readhead 1977). Assuming an optically thin spectral index of -0.7 ($F_\nu \propto \nu^\alpha$), we find $\theta_{eq} \approx 0.18$ mas. The magnetic field, then, is around 0.27 G, and the radiative lifetime is 1.3 yr. Both optically thin and optically thick models suggest very short lifetimes for the particles in the knot.

The velocity of the ejected components, if at small angles with the line of sight, can have relativistic effects that alter their apparent properties. In Figure 5 we display the range of possible true velocities for both the knot and the diffuse emission as a function of their angle of motion with respect to the line of sight; the velocities were calculated following Ginzburg and Syrovatski (1969). Since the true velocity depends on the value of Hubble's constant, we show plots for both $h = 0.5$ and $h = 1.0$, in Figures 5*a* and 5*b*, respectively. The containment of the observed emission at 2.8 cm to a cone of 20°, with the core at the apex, suggests that the central motion of the diffuse emission must be directed at an angle θ with the line of sight at least as large as the intrinsic cone width ϕ. The intrinsic cone width differs from the apparent cone width (20°) because of projection and light-travel time effects. We find that the restriction $\theta \geq \phi$ requires $\theta > 10°$ if $h = 1.0$ and $\theta > 20°$ if $h = 0.5$. In Figure 5 we have not plotted the true velocities for the diffuse component at central flow directions with angles less than these values.

The measured flux density of the knot may be Doppler-boosted above its true emission level, affecting the estimates given above for the magnetic field and radiative lifetimes in the knot. In the optically thin case, the estimate of B varies as $S^{2/7}$, where S is the flux density. In the partially optically thick scenario, $B \propto \theta^4 S^{-2}$ and $\theta \propto S^{8/17}$, so $B \propto S^{-2/17}$. If the flux density we measure is boosted above the true value by a factor X, we must change our estimate of the radiative lifetime by $X^{3/7}$ and $X^{-3/17}$, respectively. Following Ryle and Longair (1967), using $\alpha \approx +0.9$ and $\beta < 0.98$ (see Fig. 5), we find $X < 30$ if all velocity angles down to 0° are allowed. However, if one prefers to restrict the knot's motion to stay within the cone of diffuse emission, then we require its velocity angle θ to exceed 10°, and we find $X < 9.2$. The magnetic field and lifetime estimates become the following: in the optically thin case, with all angles of motion allowed, $B > 0.06h^{-2/7}$ G and $t_{life} < 13$ yr; with $\theta > 10°$, $B > 0.08h^{-2/7}$ G and $t_{life} < 8$ yr; in the partially thick case the changes in B and t_{life} are small, with B increasing to, at the most, 0.40 G and t_{life} decreasing to values on the order of 0.7 yr.

We have shown that if we assume equipartition of energy and accept the nonuniform structure model for the knot, we estimate a radiative lifetime for the knot of under 2 years. However, the knot has appeared to be relatively constant in flux throughout the 5 years of our 1.3 cm observations, and its travel time from the core at the most recent epoch is 18 years. Unless the optically thin model, with arbitrary energy spectral cutoff, is the correct model, our estimates imply that either particle reacceleration occurs in the knot or there is an excess of particle energy relative to the magnetic field energy.

The standard "central engine" models do not predict different ejection velocities that would result in the different events revealed by the knot and the diffuse component. The two components could have the same true velocities if they are moving with different inclination angles (see Fig. 5). However, different axes of ejection are probably more difficult to explain than different velocities.

The equipartition energy density estimates imply that the knot's minimum particle pressures are of order 10^{-3} dynes cm^{-2}. Such pressures could not be matched by the thermal pressure of the ambient medium through which the knot travels. However, an equal ram pressure would be possible with ambient medium densities of order 1–10 atoms cm^{-3}.

b) Models

The knot's compactness, intensity, and longevity make it a likely candidate for the hot spot model used in models of many of the superluminal sources. A hot spot could easily be incorporated into the core-jet model of Romney *et al.* (1984). The knot is unlikely to be at the end of a collimated jet, since a jet ending at the knot could not also explain the diffuse emission when the knot is much closer to the core than the diffuse emission is in the 1972–1976 2.8 cm images. The knot might be a hot spot in a moving shock or instability along a jet, such as those in M87 (Nieto and Lelievre 1982; Biretta, Owen, and Hardee 1983). The same jet could then cause the appearance of both the knot and the diffuse emission. A particularly intriguing idea is that the 1970 event resulted in an improved jet collimation efficiency while the mass flow rate in the jet stayed relatively constant, thereby producing a narrower and faster jet

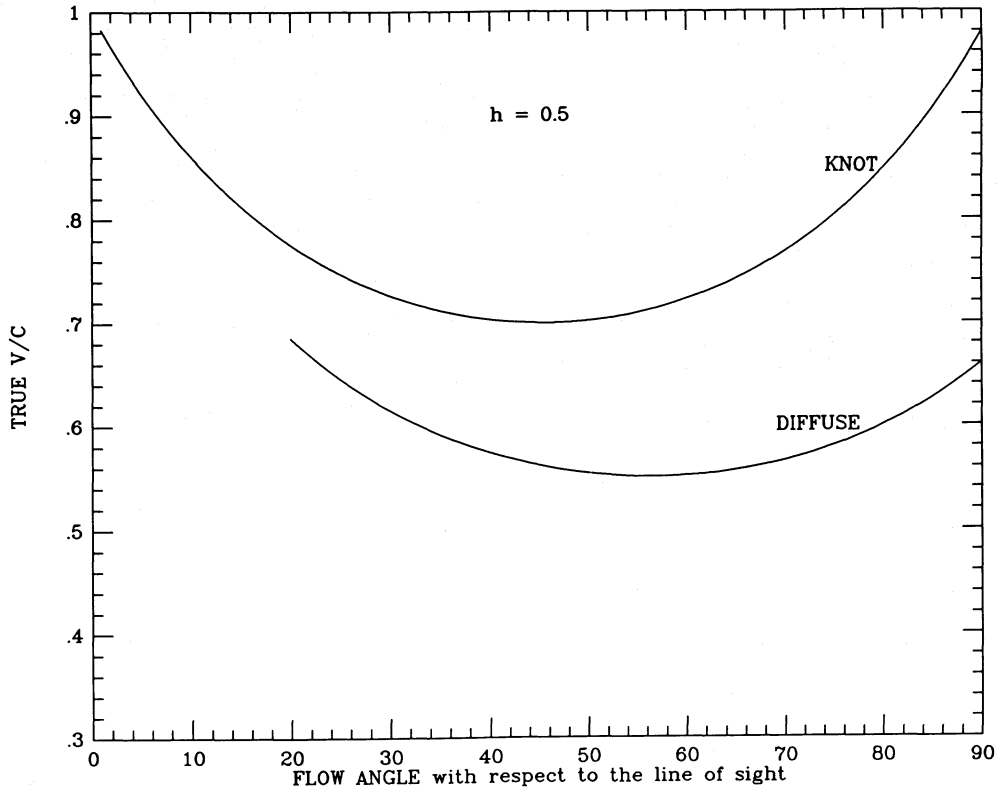

FIG. 5a

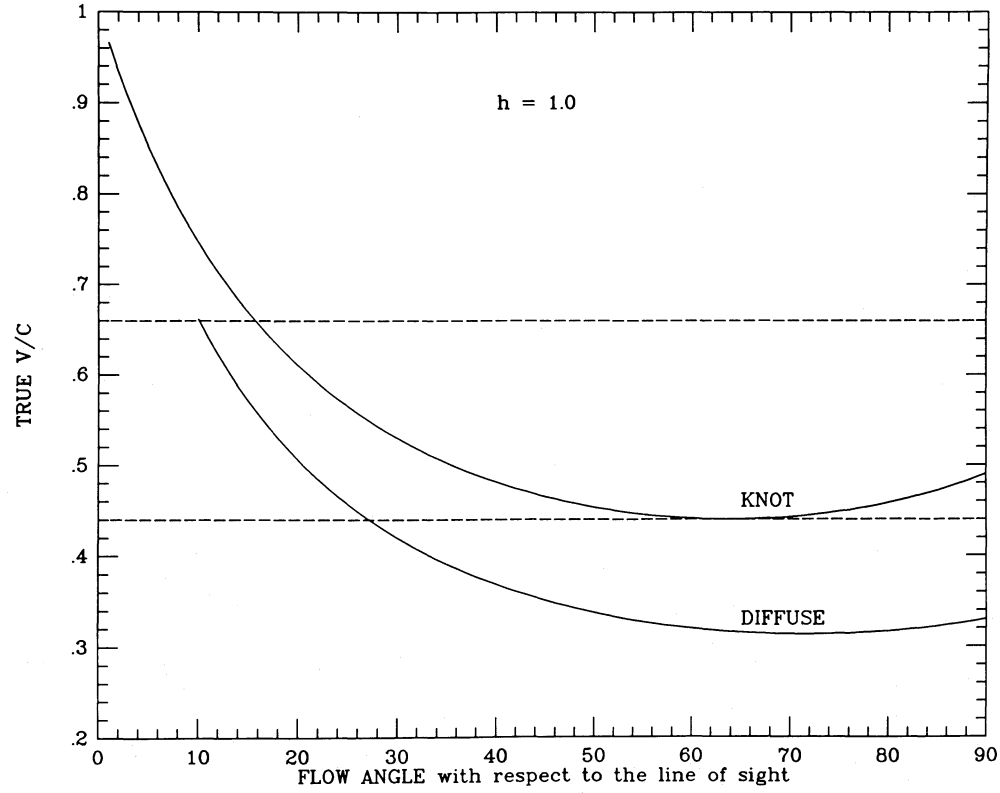

FIG. 5b

FIG. 5.—Range of possible true velocities vs. angle with the line of sight for (*a*) $h = 0.5$ and (*b*) $h = 1$ are shown. The area between the dashed horizontal lines in (*a*) shows the range of velocities that are allowed for both the knot and the diffuse component; if $H = 50$ km s^{-1} Mpc^{-1}, the knot and diffuse component could be moving at equal velocities contained within these lines.

behind a wider and slower jet. In models where particle reacceleration occurs in a jet and where jet collimation occurs outside the engine, the mass flow rate would be independent of the collimation efficiency. This situation would cause a fast-moving shock where the higher velocity ejecta impinges upon the slower ejecta ahead of it. Our maps, in this case, suggest that the jet collimation mechanism suddenly improved in efficiency about 10 years after the start of the present activity.

V. CONCLUSIONS

Our 1.3 cm VLBI observations reveal a compact, steady knot of emission moving at an apparent projected speed of $0.49h^{-1}c$. The apparent radiative lifetime of the knot is longer than that expected from minimum-energy arguments, unless particle reacceleration occurs.

Our observations, when combined with evidence from other studies, pose a strong argument for multiple and different ejection events from the same core region. The first event of recent activity occurred around 1959 and resulted in a subrelativistically expanding cone of diffuse emission and tremendous increases of flux at a wide range of radio wavelengths. The second event occurred around 1968 and resulted in a small, flat-spectrum knot of emission probably moving at a significantly higher speed than the diffuse ejecta from the previous event. The second event, also, produced a much smaller increase in the radio intensity.

We hypothesize that the second event could be associated with an increase in beam collimation efficiency, thereby producing a narrower and faster jet with the same mass transport rate behind the slower, broader jet. The surface where the faster jet impinges on the slower jet produces a shock, which causes the appearance of the knot of emission, and the velocity of the knot is faster than the speed of the slower jet.

A major flare detected at 90 and 300 GHz in 1980 indicates a third event. This event may be associated with a secondary component in the complex structure of the core region. We will report on the core structure in a subsequent paper.

We would like to thank A. P. Marscher for providing the 1984 October data, W. van Breugel for his helpful comments, T. J. Pearson and S. C. Unwin for their endless patience and help, and all the operators at the VLBI telescopes and at the Caltech correlator for their efforts. This research was partially supported by National Science Foundation grant 84-16177.

REFERENCES

Backer, D. C., *et al.* 1987, *Ap. J.*, **322**, 74.
Biretta, J. A., Owen, F. N., and Hardee, P. E. 1983, *Ap. J.*, **274**, 127.
de Bruyn, A. G. 1976, *Astr. Ap.*, **52**, 439.
Dent, W. A., O'Dea, C. P., Balonek, T. J., Hobbs, R. W., and Howard, R. J. 1983, *Nature*, **300**, 41.
Dhawan, V. 1987, Ph.D. thesis, Massachusetts Institute of Technology.
Ginzburg, V. L., and Syrovatski, S. I. 1969, *Ann. Rev. Astr. Ap.*, **7**, 375.
Marscher, A. P. 1983, *Ap. J.*, **264**, 296.
Miley, G. 1980, *Ann. Rev. Astr. Ap.*, **18**, 165.
Nieto, J.-L., and Lelievre, G. 1982, *Astr. Ap.*, **109**, 95.
Noordam, J. E., and de Bruyn, A. G. 1982, *Nature*, **299**, 597.
O'Dea, C. P., Dent, W. A., and Balonek, T. J. 1984, *Ap. J.*, **278**, 89 (ODB).
Pauliny-Toth, I. I. K., *et al.* 1976, *Nature*, **259**, 17.
Perley, R. 1986, *NRAO Newsletter*, **27**, 8.
Preuss, E., Kellermann, K. I., Pauliny-Toth, I. I. K., Witzel, A., and Shaffer, D. B. 1979, *Astr. Ap.*, **79**, 268.
Readhead, A. C. S., Hough, D. H., Ewing, M. S., Walker, R. C., and Romney, J. D. 1983, *Ap. J.*, **265**, 107.
Readhead, A. C. S., Walker, R. C., Pearson, T. J., and Cohen, M. H. 1980, *Nature*, **285**, 137.
Readhead, A. C. S., and Wilkinson, P. N. 1978, *Ap. J.*, **223**, 25.
Romney, J. D., Alef, W., Pauliny-Toth, I. I. K., Preuss, E., and Kellermann, K. I. 1982, in *IAU Symposium 97, Extragalactic Radio Sources*, ed. D. S. Heeschen and C. M. Wade (Dordrecht: Reidel), p. 291.
———. 1984, in *IAU Symposium 110, VLBI and Compact Radio Sources*, ed. R. Fanti, K. Kellermann, and G. Setti (Dordrecht: Reidel), p. 137.
Ryle, M., and Longair, M. S. 1967, *M.N.R.A.S.*, **136**, 123.
Schilizzi, R. T., Cohen, M. H., Romney, J. D., Shaffer, D. B., Kellermann, K. I., Swenson, G. W., Jr., Yen, J. L., and Rinehart, R. 1975, *Ap. J.*, **201**, 263.
Scott, M. A., and Readhead, A. C. S. 1977, *M.N.R.A.S.*, **180**, 539.
Unwin, S. C., Mutel, R. L., Phillips, R. B., and Linfield, R. P. 1982, *Ap. J.*, **256**, 83.

DONALD C. BACKER, JONATHAN M. MARR, and MEL C. H. WRIGHT: 601 Campbell Hall, Astronomy Department, University of California, Berkeley, CA 94720

RICHARD MOORE and ANTHONY C. S. READHEAD: Radio Astronomy 105-24, California Institute of Technology, Pasadena, CA 91125